



Contributions of Loading and Unloading to Overpressure: Analytical Results from The Shelfal Area of The Lower Kutai Basin, Indonesia

AGUS M. RAMDHAN and LAMBOK M. HUTASOIT

Department of Geology and Department of Groundwater Engineering, Institut Teknologi Bandung,
Jln. Ganesha 10, Bandung 40132, Indonesia

Corresponding author: agusmr@gl.itb.ac.id

Manuscript received: February, 1, 2021; revised: April, 11, 2021;
approved: June 21, 2021; available online: November, 17, 2021

Abstract - A modified Bowers Method is applied to analyze the contribution of loading and unloading to total overpressure magnitude in the shelfal area of the Lower Kutai Basin. The method combines Bowers Method with density-sonic cross plots to differentiate contributors to overpressure. This method has a strong physical background, and has proven to give satisfactory overpressure estimation in the studied area. Several processes related to overpressure and compaction in the studied area have also been deduced: 1) top of overpressure is caused by unloading due to gas generation, 2) gas generation on its own can produce overburden-scale overpressure magnitude, 3) loading starts to contribute to overpressure at depth, where the lithology is dominated by mudrocks, 4) effective stress history experienced by mudrocks before unloading, and 5) the presence of two compaction lines and therefore two associated velocity-effective stress relations.

Keywords: overpressure, loading, unloading, shelfal area, lower Kutai Basin

© IJOG - 2022.

How to cite this article:

Ramadhan, A.M. and Hutasoit, L.M., 2022. Contributions of Loading and Unloading to Overpressure: Analytical Results from The Shelfal Area of The Lower Kutai Basin, Indonesia. *Indonesian Journal on Geoscience*, 9 (1), p.1-13. DOI: [10.17014/ijog.9.1.1-13](https://doi.org/10.17014/ijog.9.1.1-13)

INTRODUCTION

In this paper, contributions of loading and unloading to total overpressure are discussed by using wireline logs in the shelfal area of the Lower Kutai Basin. Bowers Method (1995) is used in combination with cross-plot of density-sonic introduced by Dutta (2002) and Katahara (2006). Ramadhan and Goulty (2018) tried to calculate these contributions in the Bekapai Field, Lower Kutai Basin, and in this paper, our study into shelfal area of the Lower Kutai Basin is extended. Ramadhan and Goulty (2018) also used density log to estimate overpressure due to loading, and in this paper simplification is tried

by applying velocity-effective stress relation (equivalent-depth style) to the sonic log.

The shelfal area of the Lower Kutai Basin (Figure 1) is an ideal place to study overpressure and compaction for the following reasons:

1. The basin has been undergoing uninterrupted and continuous sedimentation since the Neogene, and therefore the sediments are in their maximum burial at the present time (Figure 2) (e.g. Allen and Chambers, 1998).
2. There are abundant pressure data from repeat formation tester (RFT) measurement, with some wells having over 85 RFT points (Figure 3).
3. Several wells penetrate the hard overpressure zone (overburden-scale overpressure).

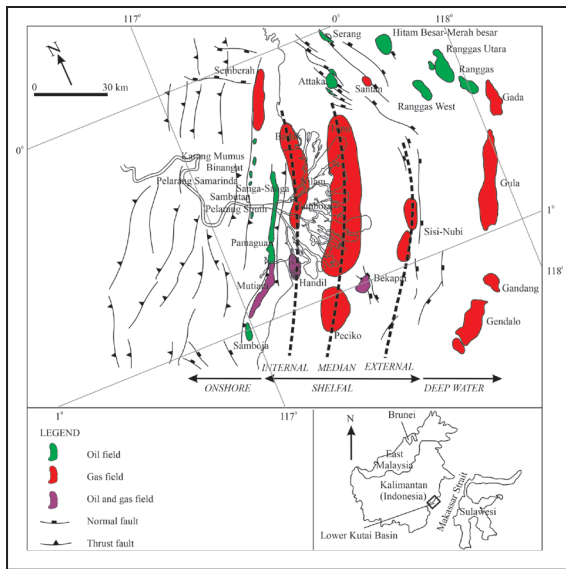


Figure 1. Outline of the Lower Kutai Basin. The location of the shelfal area is started from delta apex until series of normal faults marking boundary between shelf and deep-water area.

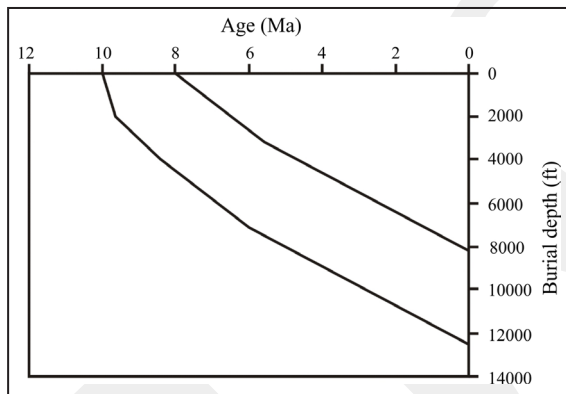


Figure 2. Typical burial history for shelfal area of the Lower Kutai Basin showing monotonously continuous sedimentation since at least 10 Ma ago.

4. Hydrocarbon maturation data in the form of vitrinite reflectance are available to analyze the relationship between overpressure and hydrocarbon generation (one of the causes of unloading overpressuring).

The results from the analysis provide new estimates of overpressure magnitude as well as new insights concerning overpressure generating mechanisms, effective stress history, and compaction behaviour of the mudrocks for the studied area of concern.

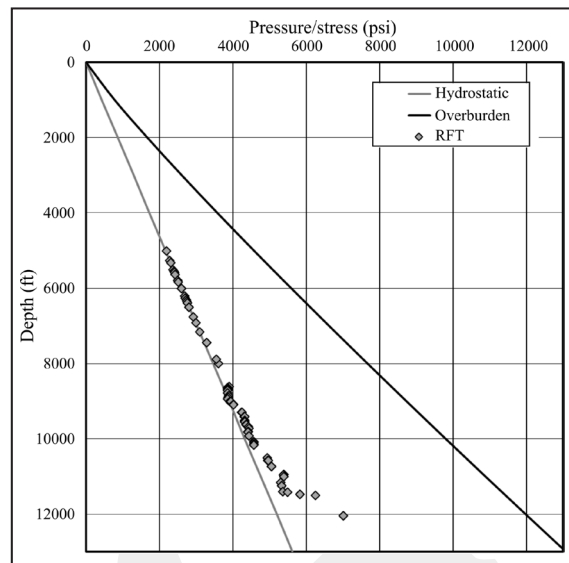


Figure 3. An example of a well data having 85 RFT points (the well is NWP-1/ Peciko Field).

METHODS

Two categories of overpressure generating mechanisms are generally considered:

1. Loading mechanism: overpressure caused by the increase in one or more principal stress unaccompanied by mudrock dewatering. This circumstance causes mudrocks fail to compact, and is commonly termed as compaction disequilibrium.
2. Unloading mechanism: overpressure caused by a decrease in effective stress due to an increase in pore fluid and/or load-bearing transfer from load-bearing material into pore fluids.

If the mudrocks are experiencing compaction disequilibrium (loading overpressuring), then their porosity will be substantially higher compared to normally compacted mudrocks (hydrostatically pressured). These higher porosity mudrocks will be reflected by lower density, higher sonic transit time (lower velocity) and lower resistivity compared to normally compacted mudrocks as illustrated in Figure 4.

If unloading then takes place, then sonic logs will indicate deflection into a much higher sonic transit time due to poroelastic effects (Figure 4). However, this poroelastic effect has a negligible

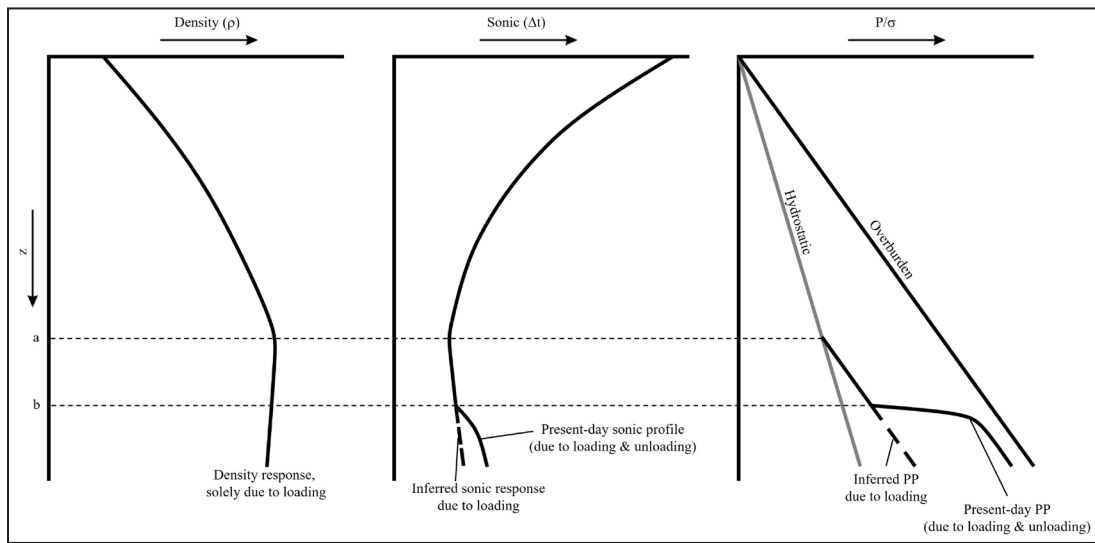


Figure 4. An illustration showing wireline log response to different overpressure mechanism. Depth 'a' is top of overpressure, and it is responded by density and sonic logs indicating that the cause of overpressure is loading. Starting at depth 'b', unloading starts to contribute to overpressure. Density only responds loading mechanism for the reason as discussed in text explanation for Figure 5. By applying density-sonic cross plot for loading, it is possible to transform density response to loading to sonic response to loading. Effective stress due to loading can be estimated from sonic response to loading by velocity (sonic reciprocal) - effective stress relation, and by knowing effective stress due to loading, estimating effective stress will be able due to loading and unloading. Pore pressure (PP) can be directly calculated by subtracting effective stress from overburden stress.

effect on density. Bowers and Katsube (2002) explained the difference between sonic and density log responses to unloading by the concept of storage pore and connecting pore (Figure 5). Storage pore is the biggest contributor to bulk porosity of the mudrock, and it is measured by density log. Meanwhile, the contribution of connecting pore to bulk porosity is negligible, but transport properties of mudrock such as sonic transit time and electric conductance are controlled by this pore type. Since unloading mostly only leads to elastic opening of connect-

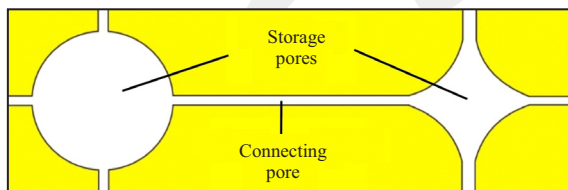


Figure 5. Pore types in mudrocks (redrawn and slightly modified from Bowers and Katsube, 2002). The biggest contributor to bulk porosity is storage pore. It is rigid, and therefore hardly affected by unloading. Connecting pore is more elastic, thus will give poroelastic response to unloading, and it is measured by sonic and resistivity logs (transport properties log).

ing pores (Hermanrud *et al.*, 1998; Bowers and Katsube, 2002), it will not have much effect on bulk porosity and therefore not significantly affect a density log. It can therefore be understood that density logs tell us more about loading, whereas sonic logs provide information about both loading and unloading.

Ramdhan and Gouly (2018) used density logs to estimate effective stress due to loading and determined pore pressures by subtraction from overburden stress (*i.e.* Terzaghi equation; Terzaghi and Peck, 1967). These data were used to determine effective stress - void ratio relationships. This technique requires an understanding of compaction parameter, β . This parameter depends on depositional age, diagenesis function, Arrhenius frequency factor, activation energy, gas constant, and temperature. In this paper, the calculation of loading overpressuring is tried to be simplified using sonic logs by applying velocity - effective stress relationships (*e.g.* Bowers, 1995). This step however requires the knowledge of sonic response to loading (dashed line in sonic log in Figure 4).

Bowers (2001) attributed sonic response to loading as maximum sonic (or velocity) that has ever been experienced by mudrocks before unloading. Sargent *et al.* (2015) and Ramdhan and Gouly (2018) coined the terminology of sonic reference trend to describe this sonic response. In this paper, this line is referred as sonic loading. The sonic loading could be constructed by applying compaction principle by means of cross-plot of density-sonic cross-plot as introduced by Dutta (2002) and Katahara (2006) (Figure 6).

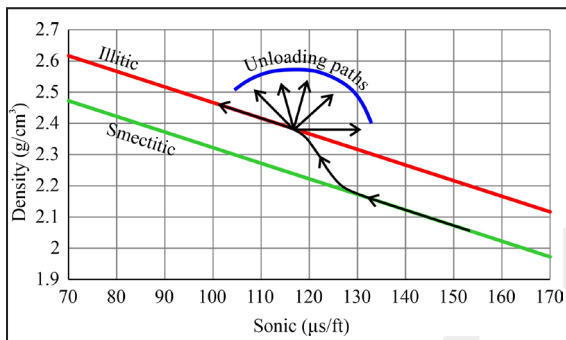


Figure 6. Cross-plot to identify the cause of overpressure. If overpressure point is located on the compaction lines (smectitic or illitic), then the cause of overpressure is loading mechanism. Unloading will push the data off the compaction trend, following blue arc (redrawn and slightly modified from Ramdhan and Gouly, 2018).

In Figure 6, there are two lines in the cross-plot, namely eodiagenesis and telodiagenesis (Dutta, 2002). Katahara (2006) added smectitic and illitic compaction trends for eodiagenesis and telodiagenesis, respectively. The equation is:

$$\rho = m\Delta t + c \dots\dots\dots(1)$$

where ρ is bulk density, Δt is sonic travel time, and m and c are regression constants.

The smectitic and illitic lines can be regarded as loading lines, *i.e.* if mudrocks experience continuous burial, the density and sonic values will follow these lines. If overpressure due to loading is present, then the data points will halt in a certain loading line (still located on the loading line). If unloading occurs, then the data points will diverge from the loading line, following curves as indicated in Figure 6 (Sargent *et al.*, 2015). By

applying the above principle, it is possible to construct sonic responses to loading by transforming density log (since density is unique to loading) using Equation (1).

Having sonic loading available, effective stress due to loading could be calculated by applying velocity – effective stress relation as given by Bowers (1995) as shown in Equation (2) below, or just simply by applying the equivalent-depth principle.

$$\sigma'_L = \left(\frac{V_L - 5000}{a} \right)^{1/b} \dots\dots\dots(2)$$

where:

- σ'_L = effective stress due to loading (psi),
- V_L = velocity response (reciprocal of sonic) due to loading (ft/s),
- a and b are regression constants.

Bowers terminology for σ'_L is maximum effective stress that has been experienced by sediments before unloaded. The resulted pore pressure due to loading can be calculated by Terzaghi Equation (3) below (Terzaghi and Peck, 1967):

$$P_L = \sigma - \sigma'_L \dots\dots\dots(3)$$

where:

- P_L = pore pressure due to loading, and
- σ = overburden stress.

In the section where unloading contributes to overpressure, the effective stress could also be calculated by applying Bowers velocity - effective stress relation for unloading with the equation as follows (Equation 4):

$$\sigma' = \sigma'_L \left(\frac{V - 5000}{V_L - 5000} \right)^U \dots\dots\dots(4)$$

- σ' = effective stress (psi),
- V = present-day velocity (from data),
- U = unloading parameter

The total pore pressure (due to loading and unloading) can also be calculated directly by subtracting effective stress from overburden stress (Equation (3)).

RESULTS

There are four typical wells analyzed in this paper, *i.e.* B-11 (Bekapai Field), NWP-9 (Peciko Field), H-9-B1 (Handil Field), and W-NB-1 (Sisi-Nubi Field). B-11 and H-9B1 penetrate very high overpressure zone, while NWP-9 and W-NB-1 were TD'ed in transition zone into very high overpressure zone. The field location can be seen in Figure 1.

B-11

Density and sonic log in mudrock section (discriminated by gamma cut-off) and pressure/stress depth plot of this well are shown in Figure 7. Density log shows density increase down to the depth $\sim 12,000$ ft, and it then reverses into lower density down to the TD of this well ($\sim 15,000$ ft). Meanwhile, sonic log starts to reverse into a higher sonic value at the depth $\sim 10,700$ ft. Pressure measurement data obtained from RFT indicate that at the depth of $\sim 10,950$ ft, the sequence has already experienced an overpressure condition.

From direct inspection of sonic log and pressure measurement data, it can be inferred that top of overpressure is located at a depth $\sim 10,700$ ft. Since density log keeps increasing starting at a depth $\sim 10,700$ ft - $12,000$ ft, it can also be de-

duced that this first appearance of overpressure is caused by an unloading mechanism. A cross-plot of density - sonic log, given in Figure 8, shows that data points diverge from the compaction line below $10,700$ ft, corroborating the interpretation that the first appearance of overpressure is due to an unloading mechanism. As discussed by Ramdhan and Gouly (2018), density reversal starting at the depth $\sim 12,000$ ft - $15,000$ ft is due to loading overpressuring. It can therefore be concluded that overpressure in the interval of $\sim 12,000$ - $15,000$ ft is caused by both loading and unloading mechanisms.

The cross-plot in Figure 8 shows smectitic and illitic compaction lines derived from the Peciko Field; the wireline log quality, especially the density log, in this field is of excellent quality. Several examples showing density - sonic relationships from the Peciko Field are shown in Figure 9. Smectitic line, transition zone, and illitic line could be observed fairly well in the figure.

A smectitic line is located at $5,000$ ft below seabed, which transitions into an illitic line at $6,000$ ft below seabed. It seems that the compaction line in B-11 is slightly lower than that of the Peciko Field. This circumstance may be caused by the differences in environmental correction of density log, mud type, temperature, or difference in mineralogy.

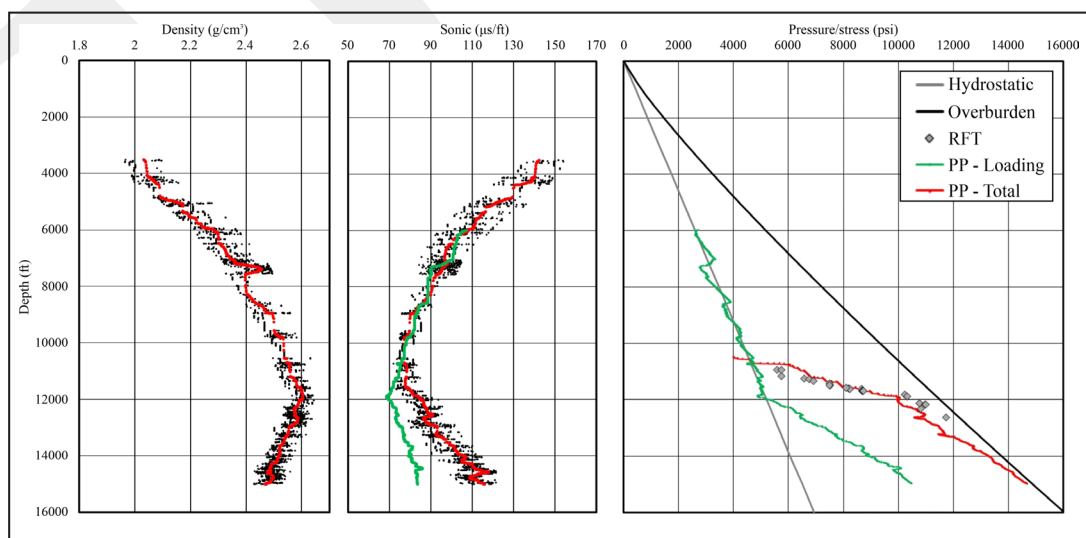


Figure 7. Wireline log responses in mudrock section to overpressure and pressure/stress plot in B-11. In the wireline log, the red line is data average (calculated by moving average with the window of 100 ft), and the green line is inferred sonic response due to loading calculated from density - sonic relation {Equation (5)}.

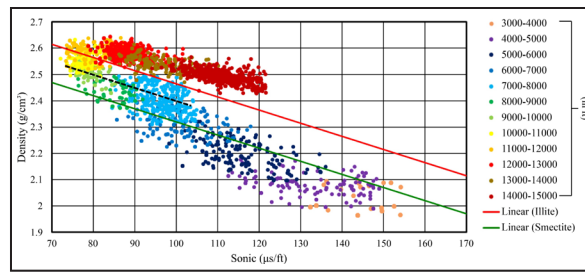


Figure 8. Density - sonic cross-plot of B-11. The black dashed line is used to construct density – sonic relation to infer sonic response to loading as given in Figure 7.

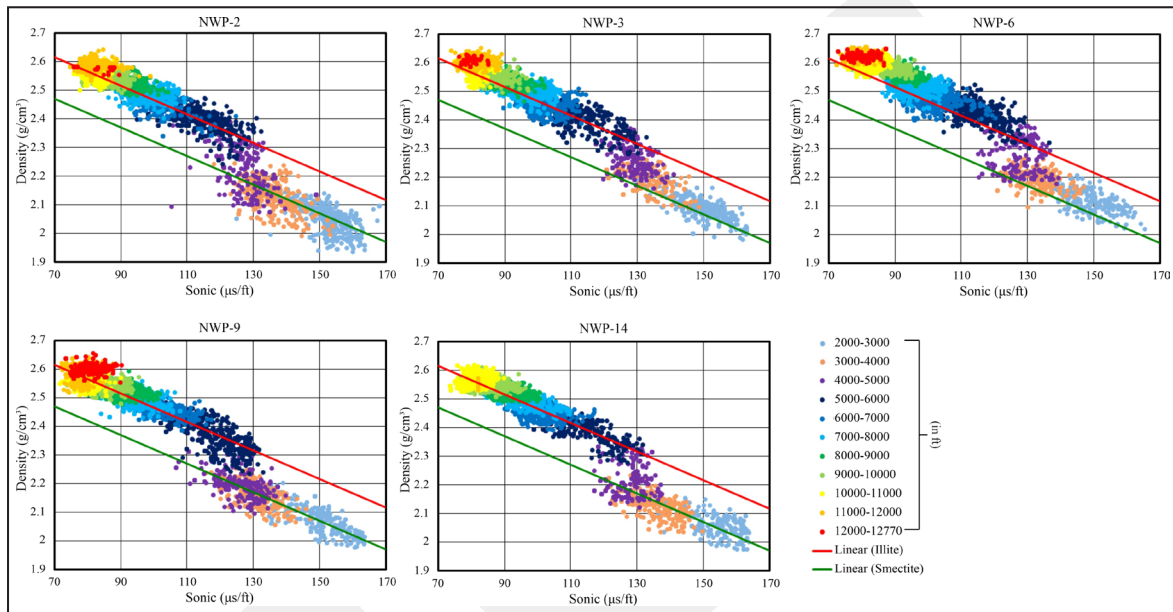


Figure 9. Density - sonic cross-plot from several wells in the Peciko Field.

As discussed in the methodology above, to estimate overpressure in this well, firstly differentiating overpressure due to loading mechanism is needed. To do so, knowing the sonic response is needed due to loading. The sonic response to loading is constructed by relating density response (since density response is only due to loading) with sonic in the section where the unloading is absent (in this case within the depth interval of 6,000 – 10,700 ft.) with Equation (1), and extrapolating over the entire overpressure section. The dashed line in Figure 8 is the section where unloading is absent, and the equation relating density and sonic is:

$$\rho = -0.0084\Delta t + 3.1958 \dots\dots\dots(5)$$

where density is in g/cm³ and sonic is in μs/ft. By extrapolating this equation over the entire

section, sonic response to loading was obtained as shown by the green line in Figure 7.

The next step is to calculate overpressure due to loading mechanism from sonic log. The sonic log used for this step is the sonic log response due to loading (green line in Figure 7). In this paper, velocity - effective stress relation was used as introduced by Bowers (1995) {Equation (2)} to calculate overpressure due to loading. This method is similar to the so-called equivalent depth method principle, *i.e.* the mudrock having the same velocity will have the same effective stress.

The velocity – effective stress relation for this well is:

$$\sigma'_L = \left(\frac{V_L - 5000}{7.5452} \right)^{1/0.81374039} \dots\dots\dots(6)$$

where:

effective stress is in psi, and velocity is in ft/s.

The effective stress estimate resulting from this step represents the maximum effective stress experienced by the sediments before unloading. In this paper, the terminology is loading effective stress. The pore pressure due to loading is obtained by subtracting loading effective stress from overburden stress. By integrating the density log equation, the overburden stress of this well can be found from (thick black line in Figure 7):

$$\sigma = 0.2263Z^{1.15381181} \dots\dots\dots(7)$$

where overburden is in psi and depth is in ft.

The resulting pore pressure due to loading is shown in Figure 7. It can be seen that overpressure due to loading increases with increasing depth. These results are very similar to the loading pressure profile previously determined by Ramdhan and Goultly (2018) from density log data using void ratio – effective stress relationships.

To calculate effective stress and total overpressure (overpressure due to loading and unloading), there are now two required parameters as shown by Equation (4), *i.e.* loading effective stress and sonic (velocity) response due to loading. The one remaining parameter, *i.e.* U (unloading parameter), is empirically chosen to match measured

pore pressure. A value of $U = 4.5$ provides good results in this context. The resulting total pore pressure is given by the red line in Figure 7. It can be seen that the chosen U value provides a good prediction of the total overpressure.

NWP-9

A similar technique as applied to B-11 is also applied to NWP-9. The density and sonic log, and pressure/stress depth plot of this well are shown in Figure 10. The density log keeps increasing with increasing depth down to the depth of ~12,000 ft. Starting from that depth down to the TD of this well (12,770 ft), the density log shows a constant value. The sonic log starts to reverse into higher sonic values at a depth ~10,700 ft, corresponding to a pressure increase observed in the pressure measurement data. Therefore, it can be inferred that the top of overpressure in this well is caused by unloading mechanism and loading starts to contribute to overpressure at the depth of 12,000 ft down to the TD of this well.

A cross-plot of density – sonic in this well indicates the occurrence of unloading is given in Figure 11. In the cross-plot, a clear shift in the compaction line from smectitic line into illitic line can also be observed, located at the depth ~5,000 – 6,000 ft.

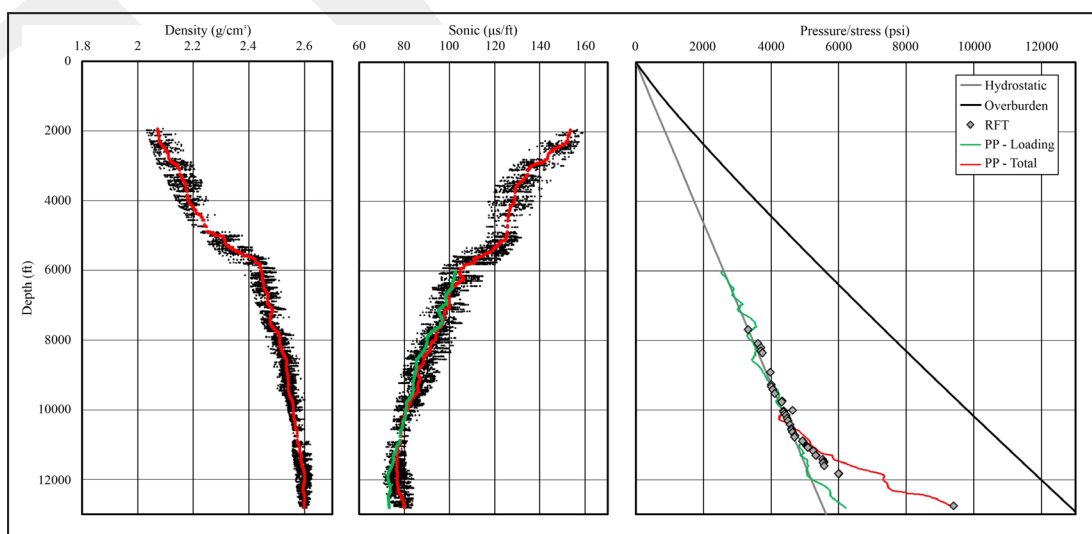


Figure 10. Wireline log responses in a mudrock section to overpressure and pressure/stress plot in NWP-9. In the wireline log, the red line is data average (calculated by moving average with the window of 100 ft.), and the green line is inferred sonic response due to loading calculated from density - sonic relation.

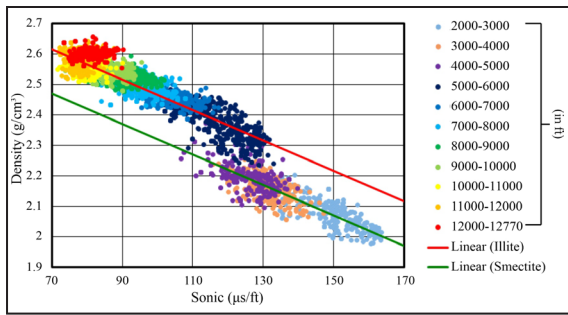


Figure 11. Density - sonic cross-plot of NWP-9.

Sonic response to loading in NWP-9 is shown as a green line in the sonic log panel in Figure 10. The resulting pore pressure due to loading is shown as a green line in the pressure/stress panel of Figure 10. The total pore pressure due to loading and unloading is given in Figure 10. A value of 4.5 was again adopted for U, which, again providing a good match between modelled and observed pore pressure data.

W-NB-1

The same technique is also applied to W-NB-1. The density and sonic logs, and pressure/stress depth plots for this well are shown in Figure 12. Similar to NWP-9, the density log keeps increasing with increasing depth down to the TD of this well indicating that there is

no contribution of loading to overpressure in this well, down to the TD. The sonic log starts to reverse into higher sonic values at a depth ~10,400 ft, corresponding to a pressure increase as observed from pressure measurement data. Therefore, it can be inferred that overpressure in this well is solely due to an unloading mechanism. Cross-plot of density – sonic in this well indicates the occurrence of unloading (see Figure 13), with a shift in the compaction line from smectitic line to illitic line, located between ~5,000 and 6,000 ft. depth.

Since there is no contribution of loading, effective stress in this well can be directly calculated by subtracting hydrostatic pore pressure from overburden stress. Meanwhile, by applying a similar technique as in B-11, sonic response to loading is shown in Figure 12 (green line). Total pore pressure due to loading and unloading is given in Figure 12. For calculating the total pore pressure, U= 4.5 is also applied, and also gives a good match between observed and modelled pore pressure.

H-9-B1

The density and sonic log, and pressure/stress depth plots of this well are shown in Figure 14. The density log interval in this well is very limit-

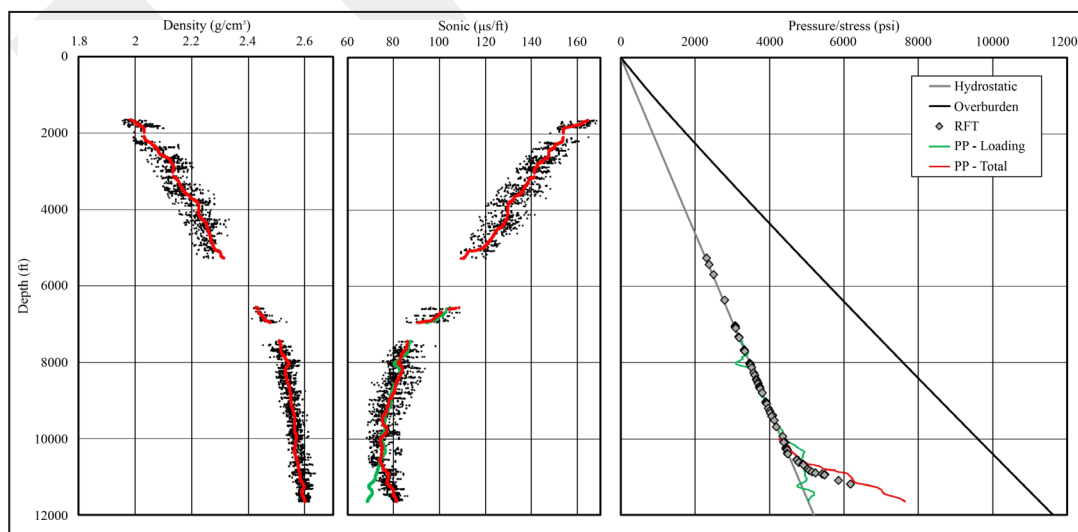


Figure 12. Wireline log responses in mudrock section to overpressure and pressure/stress plot in W-NB-1. In the wireline log, the red line is data average (calculated by moving average with the window of 100 ft), and the green line is inferred sonic response due to loading calculated from density - sonic relation.

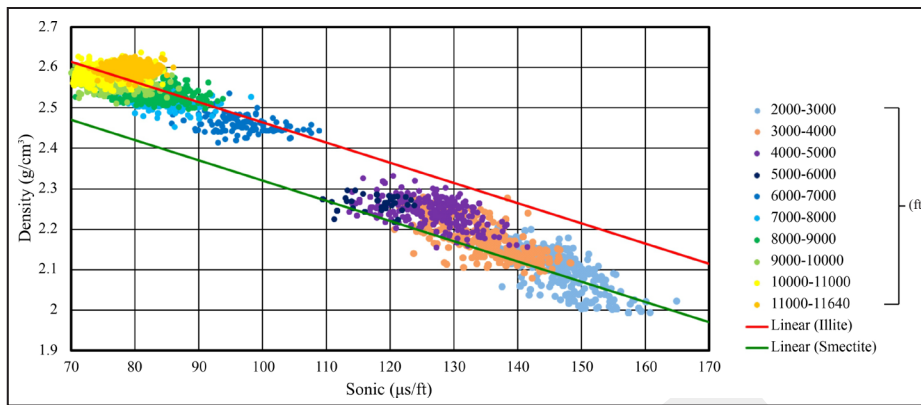


Figure 13. Density - sonic cross-plot of W-NB-1.

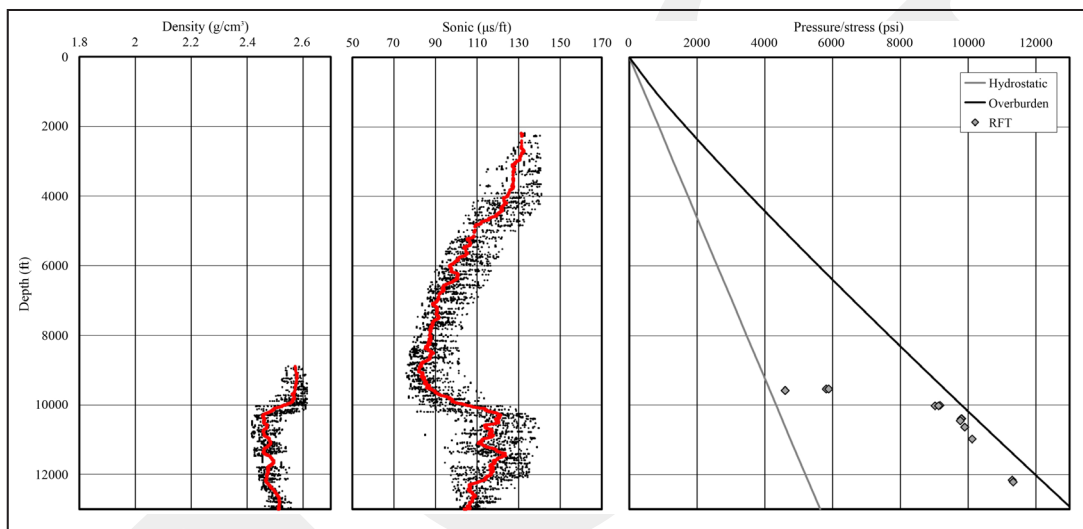


Figure 14. Wireline log responses in mudrock section to overpressure and pressure/stress plot in H-9-B1. In the wireline log, the red line is data average (calculated by moving average with the window of 100 ft).

ed, nevertheless that density starts to reverse into lower density indicating disequilibrium compaction (thus loading overpressuring) at a depth of ~10,000 ft, while sonic log starts to reverse into a higher sonic (or low velocity) at a depth ~9,400 ft. Because of the limitation of density log in this well, calculating the contribution of loading and unloading is unable in this well. However, from direct inspection, the first appearance of overpressure in this well can be interpreted to be caused by an unloading mechanism. While loading mechanism contributes to overpressure starting at a depth of ~10,000 ft down to the TD of this well. A cross-plot of density – sonic in this well indicating the occurrence of unloading is given in Figure 15.

DISCUSSION

The method discussed in this paper gives reasonably good estimates of overpressure magnitude in the shelfal area of Lower Kutai Basin. The method is semitheoretical as opposed to being purely empirical. The only empirical constant used in this method is the unloading parameter (U). Ramdhan and Goult (2018) discussed comparisons of U in several areas in the world, and found that U= 4.5 as applied in the studied area which means that sediment sensitivity to unloading is relatively low (similar to Gulf Coast and deep-water of Gulf of Mexico; Bowers, 2001). This circumstance may hinder the presence of high overpressure in sonic logs, and also seismic data for pre-drill prediction.

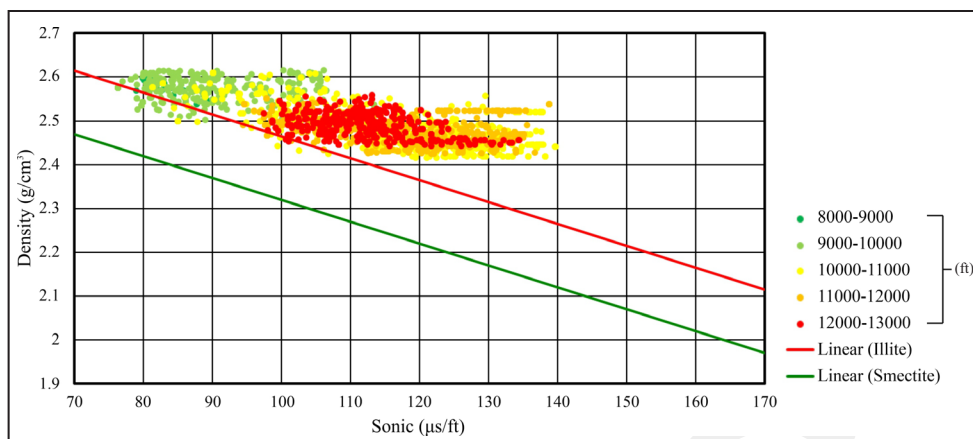


Figure 15. Density - sonic cross-plot of H-9-B1.

The technique discussed in this paper can be regarded as a modified Bowers method (Bowers, 1995). The equations used to estimate the effective stress in loading and unloading sections are taken from Bowers (1995) with additional wireline log analysis (density and sonic) taken from Dutta (2002) and Katahara (2006). The wireline log analysis is one of the key elements in this technique, since it can separate sonic response due to loading and its associated maximum effective stress (loading effective stress) {maximum ever to be experienced by sediments (sonic loading) before unloading}.

This technique also underlies the importance of density logs to estimate overpressure. By direct inspection of density log data and cross-plotting it with sonic log data, it is possible to analyze the cause of overpressure. If unloading is present, then density log is compulsory data to know sonic (or velocity) response to unloading and it is used to construct effective stress history experienced by sediments. Without density log data, it is not possible to estimate overpressure magnitude in the presence of unloading.

The dataset from the shelfal area of the Lower Kutai Basin also shows a clear shifting in compaction trend from smectitic in the shallower part to illitic in the deeper part. The transition zone is located at the depth of ~5,000 – 6,000 ft. Taking a temperature gradient of 30°C/km and seabed temperature of 30°C (see Ramdhan and Goulty, 2011), the transition zone between smectitic and

illitic line is located at the temperature of 76° - 85°C, in accordance with the temperature where smectite transforms into illite (*e.g.* Boles and Frank, 1979). The presence of two compaction lines suggests that there might be two equations describing velocity-vertical stress relation. The conventional wisdom in pore pressure prediction usually uses one single velocity-vertical stress relation for the entire section. The usage of such a technique will result in underestimation of loading overpressuring at depth.

There are two schools of thought regarding compaction in the illitic compaction line. The first school thinks that in the illitic compaction line, porosity reduction is no longer a function of effective stress (*e.g.* Bjørlykke, 1998; Hermanrud *et al.*, 1998), while the other suggests that the effective stress continues to play a role in illitic compaction (*e.g.* Sargent *et al.*, 2015). The fact that loading overpressure still takes place in the illitic line in the studied area seems to be that dataset presented here is in favour of the latter school of thought. Syaiful *et al.* (2020) who observed dataset from a Tertiary sedimentary basin in Indonesia, *i.e.* North Sumatra Basin, found that grain to grain contact can still be observed in mudrocks in illitic line, meaning that effective stress still controls porosity reduction in illitic zone. Sargent *et al.* (2015) coined the terminology of chemically-enhanced mechanical compaction for illitic compaction line to describe this porosity – effective stress dependency.

Ramdhan and Goulty (2018) discussed the possibility that density response may also be affected by unloading leading to an overestimation in overpressure. The dataset from the Lower Kutai Basin may also give additional insight on the effect of poroelastic unloading to density log. The fact that the first occurrence of overpressure in wells analyzed in this paper is responded by sonic, not by density log, shows that poroelastic unloading effect on density log is negligible. Therefore, the density reversal as observed in wells in this paper is really due to loading mechanism.

As discussed by Ramdhan and Goulty (2010, 2011, 2018), the major cause of unloading in the studied area is gas generation {see Figure 19 in Ramdhan and Goulty (2011) for example}. The vitrinite reflectance threshold for gas generation in the studied area coincides with the transition zone into high overpressure (Ramdhan and Goulty). In B-11, at the depth of ~11,800 ft, as shown by direct pressure measurement data, the magnitude of overpressure has reached very high level, close to overburden stress (overburden-scale overpressure) (Figure 7). Loading overpressure starts to operate in this well at a depth of ~12,000 ft., and therefore, overburden-scale overpressure at the depth of ~11,800 ft. is solely due to unloading caused by gas generation. It can be inferred that unloading process caused by gas generation can produce overburden-scale overpressure on its own. This is in accordance with several researchers stating that gas generation can produce very high overpressure magnitude (Swarbrick *et al.*, 2002; Hansom and Lee, 2005).

There is acknowledged uncertainty about the location of the first occurrence of overpressure, in particular whether or not it is near the prodelta mudrocks. The results confirm instead that it is located in the sequence where sand content is relatively high. Discussions in this paper may also give insight into this circumstance. Unloading overpressuring can be regarded as 'postcompaction' overpressuring, while loading overpressuring is 'syn-sedimentation overpressuring'. Therefore, the rock has already compacted (in this case mechanically and chemically), and thus the

permeability has reduced significantly, allowing a second-generation mechanism of overpressure, *i.e.* unloading, took place. This is the reason why the first appearance of overpressure in the shelfal area of the Lower Kutai Basin can be located in sand-prone sequence, because the sequence has already been compacted. Meanwhile, as it is thought previously, loading overpressuring starts to contribute to overpressure in the studied area near to the top of prodelta mudrocks, which is in accordance with conventional wisdom that loading may generate overpressure if the sequence is dominated by low permeability sequence, *i.e.* mudrock.

CONCLUSIONS

The technique described in this paper (the modified Bowers Method) has been demonstrated to provide satisfactory estimates of overpressure magnitude in the presence of complex overpressure generating mechanisms (loading and unloading) as well as describing the effective stress history experienced by mudrocks. For loading overpressuring, this technique has a robust physical basis, *i.e.* mudrocks with the same velocity will have the same effective stress (equivalent-depth principle). However, care should be taken since there might be a two velocity-effective stress relation present as observed in the shelfal area of the Lower Kutai Basin.

The technique described in this paper also shows that density log data is imperative for estimating overpressure. The density log is used to: 1) analyze the generating mechanism of overpressure, 2) differentiate the contribution of loading to overpressure, if both loading and unloading generating mechanisms are present. Without density log, it is not possible to estimate overpressure accurately.

As for the shelfal area of the Lower Kutai Basin, the usage of this technique has resolved long questions (for more than twenty-five years) about overpressuring in this area: *i.e.* about overpressure generating mechanism and the location of the top

of the overpressure region. Overpressuring in this area is quite unique, *i.e.* top of overpressure is caused by an unloading mechanism due to gas generation, while loading mechanism contributes to total overpressure at depth, in the mudrock dominated sequence (near the top of prodelta sequence). The dataset from the studied area also shows that gas generation on its own can produce overburden-scale overpressure.

ACKNOWLEDGMENTS

The authors thank Simon Mathias for thoughtful discussion and also for English proofing.

REFERENCES

- Allen, G.P. and Chambers, J.L.C., 1998. Sedimentation in the modern and Miocene Mahakam Delta. *Indonesian Petroleum Association Field Trip Guide Book*, 236pp.
- Bjørlykke, K., 1998. Clay mineral diagenesis in sedimentary basins: a key to the prediction of rock properties: examples from the North Sea Basin. *Clay Minerals*, 33, p.15-34.
- Boles, J.R. and Franks, S.G., 1979. Clay diagenesis in Wilcox sandstones of southwest Texas: implications of smectite diagenesis on sandstone cementation. *Journal of Sedimentary Petrology*, 49, p.55-70. DOI: 10.1306/212F76BC-2B24-11D7-8648000102C1865D.
- Bowers, G.L., 1995. Pore pressure estimation from velocity data: accounting for mechanisms besides undercompaction. *SPE Drilling & Completion*, p.89-95. DOI: 10.2118/27488-PA.
- Bowers, G.L., 2001. Determining an appropriate pore-pressure estimation strategy. *Offshore Technology Conference Paper*, OTC 13042, 14pp. DOI: 10.4043/13042-MS.
- Bowers, G.L. and Katsube, T.J., 2002. The role of shale pore structure on the sensitivity of wireline logs to overpressure. *In: Huffman, A.R. and Bowers, G.L. (eds.), Pressure regimes in sedimentary basins and their prediction, AAPG Memoir*, 76, p.43-60. DOI: 10.1306/M76870C5.
- Dutta, N.C., 2002. Deepwater geohazard prediction using prestack inversion of large offset P-wave data and rock model. *The Leading Edge*, 21, p.193-198. DOI: 10.1190/1.1452612.
- Hansom, J. and Lee, M-K., 2005. Effects of hydrocarbon generation, basal heat flow and sediment compaction on overpressure development: a numerical study. *Petroleum Geoscience*, 11, p.353-360. DOI: 10.1144/1354-079304-651.
- Hermanrud, C., Wensaas, L., Teige, G.M.G., Nordgård Bolås, H.M., and Hansen, S., 1998. Shale porosities from well logs on Haltenbanken (Offshore Mid-Norway) show no influence of overpressuring. *In: Law, B.E., Ulmishek, G.F., and Slavin, V.I. (eds.), Abnormal pressures in hydrocarbon environments, AAPG Memoir*, 70, p.65-87. DOI: 10.1306/M70615C4.
- Katahara, K., 2006. Overpressure and shale properties: stress unloading or smectite-illite transformation? *Expanded Abstracts 76th SEG Annual Meeting*, 25, p.1520-1524. DOI: 10.1190/1.2369809.
- Ramdhan, A.M. and Goulty, N.R., 2010. Overpressure-generating mechanisms in the Peciko Field, Lower Kutai Basin, Indonesia. *Petroleum Geoscience*, 16, p.367-376. DOI: 10.1144/1354-079309-027.
- Ramdhan, A.M. and Goulty, N.R., 2011. Overpressure and mudrock compaction in the Lower Kutai Basin, Indonesia: a radical reappraisal. *AAPG Bulletin*, 95, p.1725-1744. DOI: 10.1306/02221110094.
- Ramdhan, A.M. and Goulty, N.R., 2018. Two-step wireline log analysis of overpressure in the Bekapai Field, Lower Kutai Basin, Indonesia. *Petroleum Geoscience*, 24, p.208-217. DOI: 10.1144/petgeo2017-045.
- Sargent, C., Goulty, N.R., Cicchino, A.M.P., and Ramdhan, A.M., 2015. Budge-fudge method of pore-pressure estimation from wireline logs with application to Cretaceous mudstones at Haltenbanken. *Petroleum Geoscience*, 21, p.219-232. DOI: 10.1144/petgeo2014-088.

- Swarbrick, R.E., Osborne, M.J., and Yardley, G.S., 2002. Comparison of overpressure magnitude resulting from the main generating mechanisms. *In: Huffman, A.R. and Bowers, G.L. (eds.), Pressure regimes in sedimentary basins and their prediction. AAPG Memoir; 76, p.1-12. DOI: 10.1306/M76870C1.*
- Syaiful, M., Hutasoit, L.M., Ramdhan, A.M., and Widayat, A.H., 2020. Wireline log responses, mudweight, clay mineralogy, and implied overpressure condition: insights from Aru Field, the North Sumatra Basin. *Indonesian Journal on Geoscience, 7, p.105-119. DOI: 10.17014/ijog.7.2.105-119.*
- Terzaghi, K. and Peck, R.B., 1967. *Soil Mechanics in Engineering Practice 2nd Edition*, John Wiley & Sons, 729pp.

Preprint